Journal of Materials Chemistry A

ROYAL SOCIETY OF CHEMISTRY

PAPER

View Article Online
View Journal | View Issue

Cite this: J. Mater. Chem. A, 2021, 9, 20068

Redox-copolymers for the recovery of rare earth elements by electrochemically regenerated ion-exchange†

Haley Vapnik, ‡ Johannes Elbert ‡ and Xiao Su *

Rare earth elements (REEs) play an essential role in our modern society, being critical resources for electronic devices and renewable energy technologies. Efficient platforms for REE recovery and purification are essential to resource security and environmental management. Imparting electrochemical control over an adsorbent system can lead to higher modularity and sustainability, by enabling adsorbent regeneration without the use of additional chemicals. For the reversible capture and release of REEs, we design and synthesize a redox-copolymer, poly(ferrocenylpropyl methacrylamide-*co*-methacrylic acid) (P(FPMAm-*co*-MAA)), that combines an ion-exchange carboxyl group for REE adsorption, and a redox-active ferrocene moiety for regeneration based on electrochemical control. By molecularly tuning the copolymer composition, efficient adsorption uptake could be achieved alongside electrochemically regenerated adsorbent reuse. The copolymer electrodes exhibited an Y(III) adsorption capacity of 69.4 mg Y per g polymer, and electrochemically mediated regeneration efficiency close to 100% through oxidation of the ferrocenium units. The copolymer sorbent showed stoichiometric binding for cerium (Ce), neodymium (Nd), europium (Eu), gadolinium (Gd), and dysprosium (Dy) based on carboxyl active sites. Our work provides a proof of concept for electrochemically regenerable ion-exchange copolymers for REE recovery, and we envision generalized applications of this concept in electrifying ion-exchange systems and cation-selective separations.

Received 21st April 2021
Accepted 19th August 2021

DOI: 10.1039/d1ta03334d

rsc.li/materials-a

1. Introduction

Rare earth elements (REEs) are a group of 17 chemically similar elements consisting of 15 lanthanides plus scandium (Sc) and yttrium (Y).[1–3] The unique magnetic, phosphorescent, and catalytic properties of REEs make them irreplaceable components in a growing technology market. They play a key role in many products, from computers and smartphones to rechargeable batteries, lasers, and electric automobiles.[1,2] Over the past decades, the consumption of REEs has steadily increased due to their uses in new materials and renewable technologies.[4–12] The worldwide production of REEs has been geographically limited,[3,13] with many countries mostly relying on imported REEs from limited supply sources.[14–16] Thus, both the European Commission[17] and the U. S. Department of Energy (DOE) consider REEs to have critical supply risk, especially for neodymium (Nd), europium (Eu), terbium (Tb), dysprosium (Dy), and yttrium (Y).[18,19] With increasing demand, restricted supply, and low recycling rate, there is an urgent need for efficient REE recovery technologies.

Commonly used methods for REE separation include chemical precipitation, liquid–liquid extraction, ion-exchange, and adsorption.[20–22] However, many of these conventional approaches produce significant hazardous waste, require excess chemical input, and often have challenges in molecular selectivity.[20] Functional surfaces can be a pathway for molecular selectivity, due to the library of specific adsorption groups which have proven affinity with REEs,[20,21] including carboxyl and hydroxyl groups.[20,21,23–28] However, adsorption often requires significant chemical consumption during regeneration of adsorbent materials, including addition of acids and bases.

Electrochemical separations offer a green alternative for REE recovery, allowing for regeneration of adsorbents without the use of additional chemicals, fully promoted by electron-transfer.[29–32] Redox-active materials in particular have been shown to promote selective molecular binding.[33,34] Redox-active polymers containing ferrocenyl groups have shown high selectivity towards anionic contaminants, including metal oxyanions of arsenic and chromium, among others.[29,30,33,35–37] However, these redox-polymer platforms have mostly been restricted to applications in anion separations, with limited attention devoted to cation-selective separations. These limitations are partly due to a lack of redox-active polymers that are able to sustain

Department of Chemical and Biomolecular Engineering, University of Illinois at Urbana-Champaign, Urbana, Illinois 61801, USA. E-mail: x2su@illinois.edu

† Electronic supplementary information (ESI) available. See DOI: 10.1039/d1ta03334d

‡ These authors contributed equally to this work.

a negative charge in aqueous solutions, especially at neutral or acidic pH values. Thus, there is significant demand for functional polymer design concepts for cation-selective systems, especially for recovery of REEs and other critical elements which are often present as species with a positive charge in solution.

Recently, redox-copolymers have been used to modulate hydrophobicity and electrostatic interactions orthogonally for electrosorption of perfluoroalkyl substances (PFAS), by leveraging binding groups for PFAS with redox-active TEMPO groups for hydrophobicity and electrostatic control.[31] Unlike homopolymers, copolymers can combine different functionalities from distinct monomer units to leverage synergistic effects. Here, we propose the combination of carboxyl groups with ferrocene groups within a single redox-copolymer, to combine traditional ion-exchange effects with redox-mediated release. Poly(methacrylic acid) (PMAA) for example has been shown to efficiently adsorb metal cations by an ion exchange mechanism.[20,21,26] At the same time, polymers with ferrocene moieties in the side chain, such as poly(vinyl ferrocene) and ferrocene based (meth)acrylates, show remarkable redox properties, due to the high stability of the ferrocene (Fc)/ferrocenium (Fc^+) redox couple.[38–40]

We propose a system that combines the uptake of traditional ion exchange resins analogous to PMAA for REE capture, and regeneration by electrodesorption and charge-repulsion based on ferrocenium groups (Fig. 1). Next, we describe the synthesis and characterization of a redox copolymer, poly(-ferrocenylpropyl methacrylamide-*co*-methacrylic acid) (P(FPMAm-*co*-MAA)), and its application in the recovery of important rare-earth elements, with a focus on yttrium (Y), dysprosium (Dy), neodymium (Nd), europium (Eu), cerium (Ce), and gadolinium (Gd). We discuss the effect of different copolymer compositions on electrochemical regeneration and adsorption uptake of the REEs. This work serves as a proof of concept for electrochemically regenerated ion-exchange copolymers to enable more sustainable cation-selective separations.

2. Experimental

2.1. Synthesis and characterization of P(FPMAm-*co*-MAA)

2.1.1 Synthesis of 2-cyanovinyl ferrocene. Ferrocene carboxyaldehyde (20 g, 93 mmol) was dissolved in acetonitrile (314 g, 400 mL, 7.66 mol) and stirred in an argon atmosphere. Potassium hydroxide (5.2 g, 93 mmol) was dissolved in water (3 mL) and added to the solution. The solution was subsequently heated to reflux and stirred for 2 hours. After cooling to room temperature, the mixture was filtered, and the acetonitrile was removed under reduced pressure. The residue was dissolved in 100 mL Et_2O and washed with water. The organic phase was dried with $MgSO_4$ and the solvent removed. The crude product was recrystallized from boiling hexane (60 mL), yielding 2-cyanovinyl ferrocene (21.59 g, 91.07 mmol, 97%) as a red solid. ^{1}H NMR (400 MHz, $CDCl_3$, δ) 7.29 (d, $J = 11.8$ Hz, 1H, HCCH, *trans*), 6.98 (d, $J = 11.6$ Hz, 1H, HCCH, *cis*), 5.44 (d, $J = 16.2$ Hz, 1H, HCCH, *trans*), 5.19 (d, $J = 11.6$ Hz, 1H, HCCH, *cis*), 4.86 (t, $J = 1.9$ Hz, 2H, C_5H_4, *cis*), 4.48 (t, $J = 2.0$, 1.5 Hz, 1H, C_5H_4, *cis*), 4.47 (s, 4H, C_5H_5, *trans*), 4.21 (s, 5H, C_5H_5, *cis*), 4.21 (s, 5H, C_5H_5, *trans*). HR-ESI *m*/*z*: $[M]^+$ calcd for $C_{13}H_{11}FeN$, 237.0235; found: 237.0237. Anal. calcd for $C_{13}H_{11}FeN$: C 65.86, H 4.68, N 5.91; found: C 66.79, H 4.63, N 6.03.

2.1.2 Synthesis of 3-ferrocenyl propylamine. A hydrogenation reactor was filled with a solution of cyanovinyl ferrocene (8.0 g, 34 mmol) in ethanol (90 mL) and 30% ammonium hydroxide (30 mL). RANEY®-nickel (7.9 g, 30 wt% slurry in water, 40 mmol) was added. The reactor was closed, purged with N_2 and pressurized with hydrogen (8 bar). The reactor was

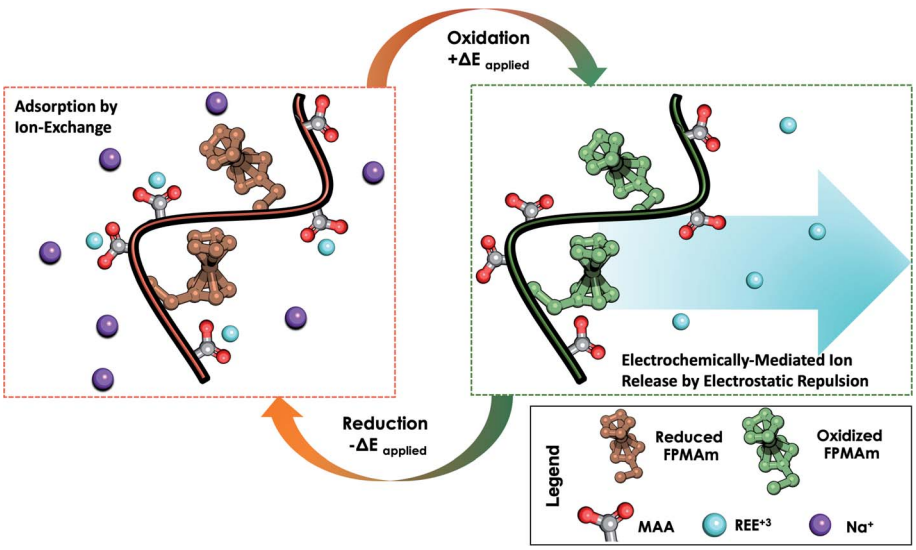

Fig. 1 Overview of the reversible capture and release of REEs by P(FPMAm-*co*-MAA) through electrochemically regenerated ion exchange. During adsorption, REE ions are captured by chemical ion exchange. During desorption, ferrocene (Fc) is oxidized to ferrocenium (Fc^+) electrochemically, allowing for desorption of the REE ions through electrostatic repulsion. Reduction of ferrocenium (Fc^+) back to ferrocene (Fc) is required for electrode cycling.

stirred at 40 °C for 4 days. The mixture was filtered through a plug of Celite to remove the catalyst, and the Celite and catalyst were washed with EtOH. The solvents were evaporated, and the residue diluted with 100 mL Et_2O. The organic phase was washed with water and brine, dried with Na_2CO_3 and the solvent evaporated. The procedure yielded 3-ferrocenyl propylamine (7.03 g, 28.9 mmol, 86%) as a red oil that was used without further purification. ^{1}H NMR (500 MHz, $CDCl_3$, δ): 4.11–4.02 (m, 9H, ferrocene), 2.72 (t, $J = 7.1$ Hz, 2H, NH_2–CH_2), 2.37 (t, $J = 7.8$ Hz, 2H, fc-CH_2), 1.66 (p, $J = 7.3$ Hz, 2H), 1.28 (s, 2H, $CH_2CH_2CH_2$). HR-ESI *m*/*z*: $[M]^+$ calcd for $C_{13}H_{17}FeN$, 243.0705; found, 243.0706. Anal. calcd for $C_{13}H_{17}FeN$. Found: C 64.22, H 7.05, N 5.76.

2.1.3 Synthesis of 3-ferrocenylpropyl methacrylamide (FPMAm). In a dry Schlenk flask with a septum, which was purged with argon, ferrocenyl propylamine (3.00 g, 12.3 mmol) was dissolved in dry dichloromethane (80 mL), and triethylamine (1.37 g, 1.89 mL, 13.6 mmol) was added. The orange solution was subsequently cooled in an ice bath and methacrylic anhydride (2.09 g, 2.02 mL, 13.6 mmol) was added slowly. After 30 min, the ice bath was removed, and the solution was stirred for another 16 h at room temperature. The reaction solution was washed consecutively with saturated aqueous $NaHCO_3$ solution, water, and brine. Afterward, the organic phase was dried with $MgSO_4$ and the solvent was evaporated after filtration. The solvent was removed, yielding the crude product as a brownish oil (4.3 g). The product was purified by flash chromatography (silica column and hexane/EtOAc gradient), yielding FPMAm (2.98 g, 9.58 mmol, 78%) as an orange solid. ^{1}H NMR (500 MHz, $CDCl_3$, δ): 5.75 (1H, broad, NH), 5.63 (s, 1H, CCH_2), 5.29 (s, 1H, CCH_2), 4.12–4.04 (9H, m, ferrocene), 3.34 (q, $J = 6.6$ Hz, 2H, $NHCH_2$), 2.40 (t, $J = 7.6$ Hz, 2H, fc-CH_2), 1.93 (s, 3H, CH_3), 1.75 (p, $J = 7.2$ Hz, 2H, CH_2-CH_2CH_2). HR-ESI *m*/*z*: $[M]^+$ calcd for $C_{17}H_{21}FeNO$, 311.0967; found, 311.0972. Anal. calcd for $C_{17}H_{21}FeNO$: C 65.61, H 6.80, N 4.50.

2.1.4 Synthesis of P(FPMAm-*co*-MAA) (P*n*). Exemplary procedure for the synthesis of P1: FPMAm (1.00 g, 3.21 mmol), methacrylic acid (277 mg, 3.21 mmol) and AIBN (10.5 mg, 0.06 mmol) were dissolved in 1,4-dioxane (4 mL). The mixture was degassed by bubbling with argon for 15 min and heated to 60 °C for 16 h. The polymer was precipitated in diethyl ether (50 mL) and filtered. The polymer was dissolved in 25 mL of THF, precipitated again in diethyl ether and dried under reduced pressure, yielding 1.11 g (87%) P($FPMAm_{44}$-*co*-MAA_{56}) (P1) as an orange solid. GPC: $M_n = 9.5$ kg mol^{-1}, $M_w = 31.4$ kg mol^{-1}, $Đ = 3.29$.

2.1.5 Synthesis of P(BzMA-*co*-MAA) (P5). BzMA (2.00 g, 11.35 mmol), methacrylic acid (977 mg, 11.35 mmol) and AIBN (37.3 mg, 0.23 mmol) were dissolved in 1,4-dioxane (15 mL). The mixture was degassed by bubbling with argon for 15 min and heated to 60 °C for 16 h. The polymer was precipitated in acetonitrile (50 mL) and filtered. The polymer was dissolved in 25 mL of THF, precipitated again in acetonitrile and dried under reduced pressure, yielding 1.95 g (78%) P($BzMA_{52}$-*co*-MAA_{48}) as a colorless solid.

2.2. Preparation of P(FPMAm-*co*-MAA)-CNT electrodes

To fabricate immobilized ferrocene electrodes, two stocks were prepared: stock A consisting of 12 mg of P(FPMAm-*co*-MAA) (P1) in 3 mL of deionized (DI) water and 60 μL of 1 M NaOH, and stock B consisting of 12 mg of CNT (multiwalled carbon nanotubes), 1.2 mg of 1,3-BDSA in 1.5 mL of dimethylformamide (DMF). Stock A was stirred and heated until the polymer was fully dissolved while stock B was sonicated for 30 min in ice water. P1/CNT (1 : 1 ratio) was prepared by mixing stocks A and B and sonicating for 4 h in an ice-bath. Once prepared, a titanium-grade 1 mesh (titanium screen, Fuel Cell Store) cut into rectangles (1 cm × 2 cm, 53 μm thick) was drop-coated with the solution containing the active material, with about 40–50 μL for each drop, and left to dry at 95 °C in an oven between drops, with a final total coated area of active material of 1 cm^2. After coating, the polymer-coated electrodes were left overnight to ensure that all solvent was evaporated. The electrodes were left in an oven at 140 °C for 3 h to activate the crosslinker. Total coating mass was determined by the weight difference of the substrate before and after coating in a high-accuracy analytical balance. The coated electrodes were then connected to a copper wire with copper tape. These functionalized electrodes with the P1 polymer will be referred to as P1-CNT. Electrodes coated with other materials used in this paper were assembled in the same fashion as P1-CNT electrodes with some having variations to the coating solutions. Further details on materials and instruments for characterization can be found in Section SI-1,† and detailed electrode preparation is presented in Section SI-2.†

2.3. Adsorption experiments

2.3.1 Equilibrium adsorption tests. Batch adsorption experiments were primarily carried out with yttrium(III) to determine performance and adsorption parameters, with Y(III) being used as the model for REE ions in this system for the proof of concept. We then evaluated our electrodes for neodymium (Nd), europium (Eu), gadolinium (Gd), dysprosium (Dy), and cerium (Ce) to demonstrate the generality in the concept. Stock solutions were prepared by dissolving $RECl_3$ and NaCl salts in deionized (DI) water. Solutions were prepared containing 1 mM YCl_3 and 20 mM NaCl in DI water ($NdCl_3$, $EuCl_3$, $GdCl_3$, $DyCl_3$, or $CeCl_3$ replacing YCl_3 when applicable), with the REE as the minority ion in twenty-fold higher competing cation concentration to mimic brackish industrial and mining wastewater conditions. In addition, the effect of ionic strength was also tested by varying the concentration of NaCl from 5 to 100 mM. All adsorption tests were performed with a titanium (Ti) coated electrode in 10 mL of stock solution and stirred at 300 rpm at room temperature. Experiments were run for 1 h unless otherwise stated. The initial and final concentrations of the REE solutions were determined using ICP-OES (5110 ICP-OES, Agilent Technologies). Samples were run through the ICP in 10 replicates, with each experiment solution measured in triplicate and each experiment repeated at least twice. The concentration of the stock solution used for each experiment was determined by ICP in the same run as the correlating experiment to allow for identical ICP conditions

when comparing initial and final concentrations. The uptake values are reported as the adsorption capacity normalized by the mass of the total coating (polymer + CNT + cross-linker per electrode, unless otherwise stated). Adsorption capacity was determined using eqn (1):

$$q = \frac{(C_0 - C) \times V}{m} \quad (1)$$

where q is the adsorption capacity (mg g^{-1}), C_0 and C are the initial and final REE ion concentrations (mg L^{-1}), V is the volume of the solution (L), and m is the mass of the electrode coating (g).

2.3.2 Effects of solution pH on REE adsorption. The effect of pH on adsorption capacity was investigated by adjusting a solution of 1 mM YCl_3 and 20 mM NaCl to the desired pH values using either dilute HCl or NaOH solution. The initial and final concentrations of REEs were determined in the same manner as mentioned earlier, where the corresponding stock with the specifically tested pH was compared to the solution in the experiment with the same initial pH level.

2.3.3 Adsorption kinetics and equilibrium isotherm. Kinetics were measured with the P1-CNT electrode placed in an Y(III) stock solution (10 mL of 1 mM YCl_3 and 20 mM NaCl, pH = 6). The equilibrium isotherm was measured at different initial concentrations (10 mL of 0.1–3.0 mM YCl_3 and 20 mM NaCl, pH = 6) and stirred at 300 rpm at room temperature for 1 h.

2.3.4 Adsorption selectivity. The REE stocks used in single REE adsorption tests contained 20 mM NaCl. XPS spectra were used to compare the uptake of REE ions and Na ions when using P1-CNT electrodes. The electrodes examined were placed in 10 mL of aqueous solution containing 1 mM YCl_3 and 20 mM NaCl for 1 h. Selectivity between selected REE ions was also tested by assaying each sample for all the REEs before and after adsorption. 10 mL of a solution containing a mixture of Y(III) and Ce(III), and 10 mL of a solution containing a mixture of Y(III) and Dy(III), at a concentration of 1 mM each, were tested.

2.4. Electrochemically mediated regeneration

For desorption tests, 10 mL of solution with a background electrolyte concentration of 20 mM NaCl was used. Chronoamperometry was used for all desorption tests in this work. ICP-OES was used to determine the amount of REE ions desorbed into solution. The electrode regeneration experiments were carried out similarly with Y(III) as the model REE ion. After electrochemical desorption, the P1-CNT was reduced to neutralize the positive charge and reuse the electrode for cation adsorption. Chronopotentiometry was used for electrode reduction steps, with an applied current of −0.025 mA under a nitrogen purge (procedure optimized after trial and error). The electrodes could then be subsequently used for further adsorption/desorption cycles.

3. Results and discussion

3.1. Synthesis and characterization of P(FPMAm-*co*-MAA)

To overcome the challenge of regeneration of traditional carboxylic acid-based adsorbents for REEs, we aimed to combine the carboxylic acid moiety with a redox-active ferrocene moiety in a copolymer. The electrochemical oxidation of the neutral ferrocene to the positively charged ferrocenium ion should introduce enough positive charges on the polymer to compensate for the negative charges of the carboxylate anions, and consequently displace the REE cations once bound. To achieve this goal, methacrylic acid (MAA) was chosen as the carboxylic acid monomer, due to its large-scale commercial availability and low cost. Ferrocenylpropyl methacrylamide (FPMAm) was chosen as the ferrocene-containing monomer, because it has been proven to have a remarkable cycling stability in aqueous redox flow batteries and does not have the limitations of vinyl ferrocene in a free radical polymerization process.[40–42]

The synthesis of FPMAm starting from ferrocene (Scheme 1) was improved to increase the overall yield from 51%, reported previously,[40] to 65%. The limitation of the previous synthesis was the reduction of the nitrile to the amine with LiAlH with a yield of only 60%. By combining this step and the hydrogenation of the C=C double bond into a single hydrogenation step using RANEY®-nickel as the catalyst, the yield was improved to 86% and the synthesis shortened by a whole step. Further improvements were achieved by replacing the time and resource intensive chromatographic purification of the 2-cyanovinyl ferrocene with a simple recrystallization protocol and replacing the expensive methacryloyl chloride with much cheaper methacrylic anhydride for the last step of the synthesis. FPMAm and MAA were copolymerized by free radical copolymerization (Scheme 2), yielding a copolymer with different ratios of FPMAm and MAA and thus different ratios of sites for REE binding and redox-active groups.

The ratio of monomers determined by ^{1}H NMR spectroscopy and the P(FPMAm$_x$-*co*-MAA$_{100-x}$) used in this study are summarized in Table 1, with x indicating the content of FPMAm in mol%. Furthermore, a copolymer of MAA and hydrophobic benzyl methacrylate (P(BzMA$_{52}$-MAA$_{48}$)) was synthesized as a non-redox active control. Measurement of the molecular weight was attempted by gel permeation chromatography, and only the polymer with low MAA content (P2) yielded consistent results (Fig. S28†). The polymer with a higher MAA content (P1) formed micelles in DMF, as shown by dynamic light scattering (DLS) measurements. This micellization was due to the high content of carboxylate groups, which are not well solubilized in DMF, and the organosoluble FPMAm repeating units stabilizing the micelles. When P1 was dissolved in water it also formed micelles with the hydrophobic ferrocene moieties forming the core of the micelles.

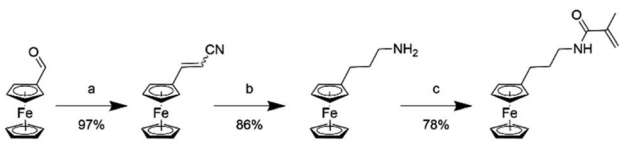

Scheme 1 Synthesis of the FPMAm monomer: (a) acetonitrile/water, KOH, reflux, 2 h; (b) RANEY®-nickel, H_2 at 8 bar, NH_4OH, EtOH, 40 °C, 4 days; (c) methacrylic anhydride, NEt_3, CH_2Cl_2, 0 °C, 16 h.

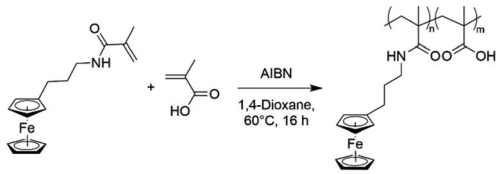

Scheme 2 Free-radical copolymerization of FPMAm with MAA to yield P(FPMAm-*co*-MAA).

Table 1 Overview of the copolymer composition

	Monomer ratio [mol% FPMAm]	
	Target[a]	Measured[b]
$P(FPMAm_{44}\text{-}co\text{-}MAA_{56})$ (P1)	50	44
$P(FPMAm_{69}\text{-}co\text{-}MAA_{31})$ (P2)	70	69
$P(FPMAm_{26}\text{-}co\text{-}MAA_{74})$ (P3)	30	26
PFPMAm (P4)	100	100
$P(BzMA_{52}\text{-}MAA_{48})$ (P5)	50[c]	52[c]

[a] Targeted monomer ratio at the start of the reaction. [b] The FPMAm content was determined by ^{1}H NMR spectroscopy. [c] Mol% BzMA.

3.2. Fabrication and characterization of P(FPMAm-*co*-MAA)-CNT electrodes

The main challenge in the fabrication of stable electrodes for use in water is the water solubility of the polymers – especially in the oxidized state. To prevent dissolution of the polymer, crosslinking of the polymer film was performed. 1,3-Benzenedisulfonyl azide (1,3-BDSA) was used as a crosslinker. By heating to temperatures > 120 °C, the sulfonyl azide groups of this crosslinker formed reactive nitrene species that inserted into the C–H bonds of the polymer, thus crosslinking the polymer.[43] Without the crosslinker, P1 was seen to quickly dissolve out of the P1-CNT electrodes due to the water solubility of PMAA (Fig. S1a†).

The stability and redox activity of the P1-CNT electrode was investigated using cyclic voltammetry (CV) (Section SI-3†). Redox activity in the redox-copolymer was confirmed through CVs, with clear reversible oxidation and reduction of the ferrocenyl groups observed (Fig. 2). Crosslinking with 1,3-BDSA was used to prevent P1 (and the other MAA containing polymers) from dissolving into the aqueous solution and therefore stabilize the P1-CNT electrodes. The ratios of cross-linking reagent/P1 tested were 0, 0.05, 0.1, and 0.2 wt%. Even with crosslinking, the P1-CNT electrodes display some initial loss of active material due to incomplete crosslinking. However, the charge of the electrodes stabilized quickly and led to a stable operational charge of ~80% of the initial charge. On the other hand, the polymer in the P1-CNT electrode without crosslinking quickly dissolved completely (Fig. S1 and S2†), showing the importance of optimizing crosslinking compositions. The optimal ratio of cross-linking reagent/P1 (and all polymers containing MAA) of 0.1 wt% was used throughout the rest of the work. The elemental mapping images of the P1-CNT electrode were recorded, and its surface morphology was examined (Fig. S7 and Table S3a†) to confirm the stability of the polymer in the coating and also show the microporous morphology of the electrode.

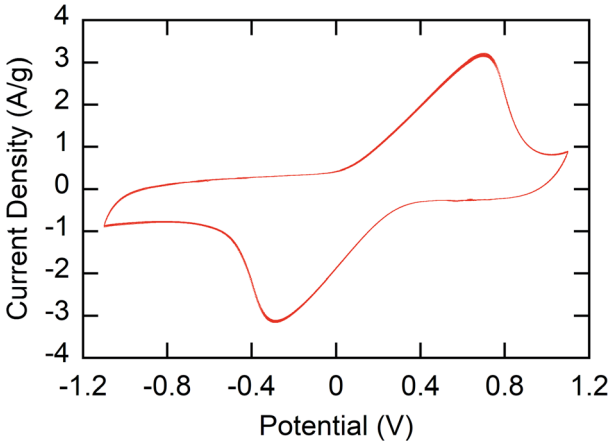

Fig. 2 Cyclic voltammetry of the P1-CNT/Ti electrode's final 10 cycles (from over 100 cycles) in the presence of 100 mM $NaClO_4$. The potential range chosen was from −1.1 to 1.1 V with a scan rate of 50 mV s^{-1}.

3.3. REE adsorption

3.3.1 Investigation of the polymer structure and target REE screening. Adsorption experiments for Y, and additional Na ions, were performed on several different adsorbents, including P(FPMAm)-CNT (ferrocene functional group control), $P(FPMAm_{70}\text{-}co\text{-}MAA_{30})$-CNT, $P(FPMAm_{25}\text{-}co\text{-}MAA_{75})$-CNT, and $P(BzMA_{52}\text{-}MAA_{48})$-CNT (non-redox active control), as well as just CNT, to evaluate the effect of the polymer structure. All tests for all adsorbents and all REEs were performed under the same conditions (10 mL of aqueous solution containing 1 mM $RE(Cl)_3$ and 20 mM NaCl, 1 h run time, open circuit, pH of 6, at room temperature).

Based on experimental results (Fig. 3a), the Y ion uptake increased with increasing methacrylic acid content in carboxylic acid moieties. Negligible Y uptake was observed on electrodes coated with the active material without carboxylic acid groups (P(FPMAm)-CNT and CNT controls), providing strong evidence that carboxylic acid moieties were solely responsible for Y interaction, and the ferrocenyl groups and CNT provided little to no uptake by themselves, and there was no secondary adsorption onto the experimental setup itself. The concentration drop of Y (in ppm) for all the controls is summarized in Section SI-17.† The ratio of Y ion uptake to carboxyl adsorption sites (Fig. 3b) was close to the theoretical value of 1/3 for the formation of a $RE(RCOO)_3$ complex, showing the high accessibility and utilization of the redox-copolymer adsorption sites. A detailed description of the adsorption site calculation is given in Section SI-6.† P1 and $P(FPMAm_{70}\text{-}co\text{-}MAA_{30})$ (P2) have utilized most REE binding sites within 1 h. $P(FPMAm_{26}\text{-}co\text{-}MAA_{74})$ (P3) showed a slightly lower binding site utilization. This could either indicate a slower adsorption kinetics or be

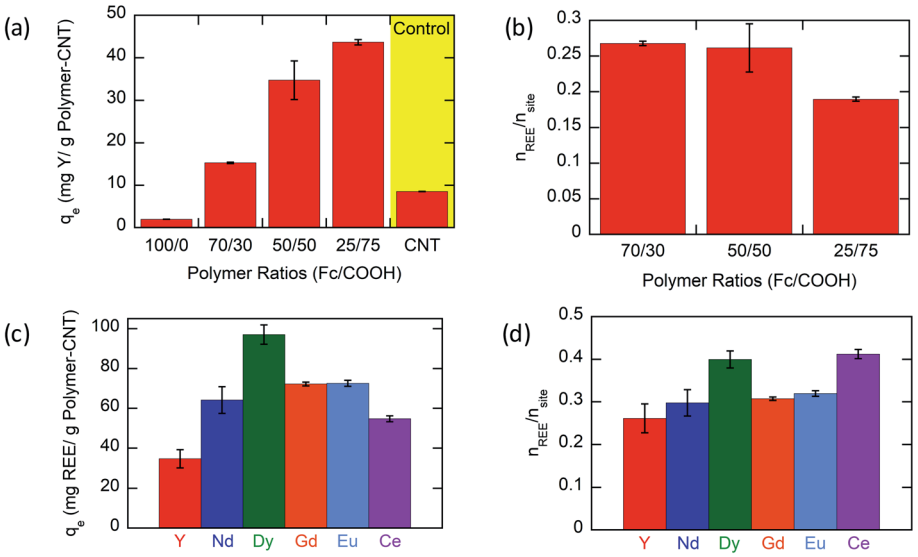

Fig. 3 The removal of REE ions. Running conditions are as follows: 1 h, open circuit, 10 mL aqueous solution with 1 mM $RE(Cl)_3$ and 20 mM NaCl. (a) Uptake of Y(III) onto polymer-CNT/Ti electrodes, with copolymers of various ratios of ferrocenyl groups to carboxylic acid groups (with the control being CNT/Ti electrodes without any polymer). (b) Number of Y(III) moieties adsorbed to the number of available adsorption sites (carboxylic acid sites) on polymer-CNT (P1-CNT) electrodes with polymers having various ratios of ferrocenyl groups to carboxylic acid groups. (c) Uptake of various REEs using P1-CNT. (d) Ratio of RE(III) adsorbed to the available adsorption sites based on carboxylic acid units in the polymer.

attributed to increased steric or coulombic interactions. Adsorption experiments of REEs of interest (Y, Nd, Eu, Gd, Dy, and Ce) with Na ions were performed on P1-CNT electrodes. Nd, Eu, Gd, Dy, and Ce were tested under the same conditions as yttrium (10 mL of aqueous solution containing 1 mM $RE(Cl)_3$ and 20 mM NaCl, 1 h run time, open circuit, pH of 6, room temperature). All REEs tested showed significant uptake using P1-CNT (Fig. 3c), with the ion to adsorption site ratio close to 1/3 as well (Fig. 3d), indicating similar mechanisms for these trivalent cations. For Dy and Ce, there was a higher ratio of adsorbed REE ions per adsorption site, indicating that fewer carboxylic acid groups were binding each cation, which may hint at other possible coordination geometries at play with these two elements. Further investigation of the ligand binding mechanisms will be carried out in future work for these elements.

The influence of ionic strength was investigated to evaluate various aqueous conditions in practical applications. The effect of ionic strength on the adsorption of Y(III) was tested at various initial concentrations of NaCl from 5 to 100 mM. As shown in Fig. S31,† the adsorption capacity decreases at higher concentrations of Na^+, but the degree of reduction is extremely small. These results show that Y(III) has a stronger binding force than Na^+ for the adsorption sites and that P1-CNT electrodes can be used to remove REEs from aqueous waste streams containing various amounts of salt.

3.3.2 Effect of solution pH. The pH of the solution is a major factor affecting the degree of protonation, and thus the adsorption capacity of carboxylic acid-based adsorbents. The effect of pH on the adsorption of Y(III) was investigated in a pH range of 2–7. Precipitation of insoluble REE hydroxides at pH above 7 limits the usability under basic conditions. The adsorption of Y(III) on P1-CNT had a strong pH-dependence, as shown in Fig. 4a. There was little to no Y(III) adsorption for pH < 4 since the carboxylic acid groups are fully protonated at low pH and the pK_a of free PMAA is around 4.7.[44] Increasing the pH resulted in deprotonation of the adsorbent, and therefore led to an increase in active adsorption sites available for REE cations. The highest uptake was observed at pH 6, which is the pH of the unadjusted solution used for all other experiments (adsorption capacity of 34.7 mg Y per g P1-CNT). The distribution coefficient (K_d) was also calculated for different pH values and is shown in Section SI-19.† The pH for both adsorption and electrochemical release was measured and is reported in Table S5.† For both sorption and release cases, the pH change is very limited, which emphasises that pH changes do not play a major role in adsorption or regeneration performance.

3.3.3 Adsorption kinetics. To measure the kinetics of Y(III) adsorption over the P1-CNT electrode, the adsorption was monitored at different contact times from 0 to 24 h, as shown in Fig. 4b. The adsorption capacity was shown to reach equilibrium within 60 min. To evaluate the adsorption process of Y(III) for P1-CNT electrodes, pseudo-first-order (PFO) and pseudo-second-order (PSO) kinetic models were used to fit the experimental kinetic data. A detailed description of the kinetic models is given in Section SI-4,† with fitted plots presented in Fig. S3 and S4.† The parameters of the PFO and PSO models and the correlation coefficients (R^2) estimated using the two models are given in Table S1.† [45]

3.3.4 Adsorption isotherms. The adsorption data were fitted with Langmuir or Freundlich isotherms.[46–48] A detailed description of the isotherm models is given in Section SI-5,†

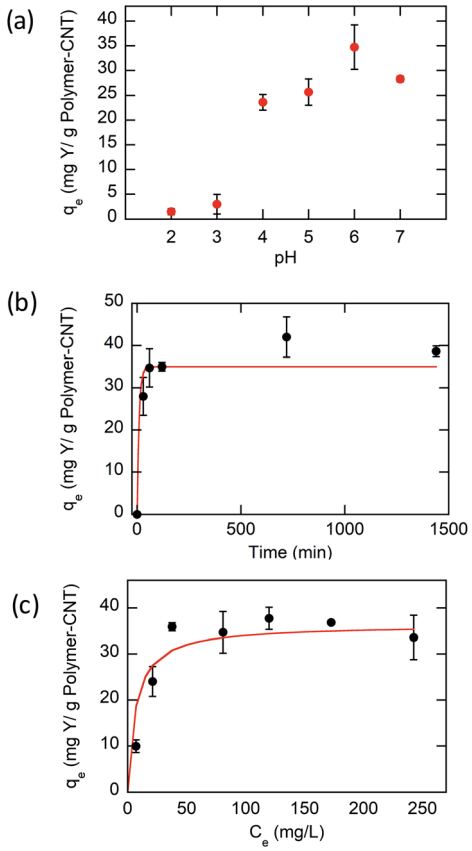

Fig. 4 (a) Effect of pH on Y(III) adsorption uptake on P1-CNT. (b) Kinetic data and pseudo-first-order model for the adsorption. (c) Adsorption isotherm and Langmuir fit line of Y(III) adsorption on P1-CNT.

with fitted plots presented in Fig. S5 and S6.† The obtained isotherm constants, fitted to the two models for Y(III) adsorption isotherms of P1, are summarized in Table S2.† The redox-copolymers display Langmuir adsorption behaviour, as shown in Fig. 4c, reflecting a site-based adsorption model ($R^2 = 0.987$).

3.3.5 Adsorption selectivity. Adsorption selectivity was evaluated through the relative separation factor (RSF) between the target elements, defined by

$$\mathrm{RSF}_{A/B} = \frac{([A]/[B])_{ads}}{([A]/[B])_{sol}} \quad (2)$$

where $([A]/[B])_{ads}$ is the ratio of the two competing ions that are adsorbed and $([A]/[B])_{sol}$ is the ratio of the two competing ions present in the aqueous solution at equilibrium adsorption. RSF values greater than 1 indicate higher selectivity of A compared to B, while RSF values less than 1 indicate higher selectivity of B compared to A. The selectivity of P1-CNT was screened for Y(III) against Na^+ ions. P1-CNT was immersed in an aqueous solution, containing 1 mM $RE(Cl)_3$ and 20 mM NaCl, for 1 h. Table 2 shows the RSF obtained using P1-CNT, where XPS and ICP analysis were used to calculate the adsorbed ion ratio. The final concentration of NaCl in solution is assumed to have no significant change from the initial values due to the high solution concentration levels compared to its uptake. Even with a higher concentration of Na^+, the REE ions showed a stronger binding to the adsorption sites, following the expected behaviour of these selective anionic ligands. These results indicated that P1-CNT could remove REEs in the presence of a significant excess of competing ions. Selectivity of P1-CNT between REEs also was investigated through competitive adsorption tests with Y *vs.* Ce and Y *vs.* Dy. For these competitive adsorptions, we used 1 h contact time in 10 mL aqueous solution, with 1 mM for each of the REE salts (and without competing NaCl). The RSF values for Y/Ce and Y/Dy, obtained using ICP measurements, are shown in Table 2. The carboxylic acid ligands serve as the models for the proof of concept in the current work, with future incorporation of more selective ligands between REEs being equally flexible through the synthetic pathways presented above.

3.4. Redox-mediated regeneration and cycling

Most importantly, we evaluate the electrochemical regeneration of our redox-copolymer systems for the bound REEs. In practical column adsorption applications, stripping of adsorbed ions is required for reuse of the adsorbent in the subsequent adsorption. While traditional ion exchange resins require stripping with a strong acid or base, thus generating an additional hazardous and corrosive waste stream, our proposed combination of carboxylic acid and redox active ferrocene moieties within a single copolymer allows for solely electrochemically controlled regeneration of the adsorbent. Compared to traditional adsorbents, our electrochemical approach only requires electricity for desorption, thus eliminating the need for highly acidic or alkaline stripping reagents. Bound REE ions can be released into solution through electrostatic repulsion of the positively charged ferrocenium ions, through electrochemically driven oxidation. The electrosorption of REE loaded P1-CNT electrodes was investigated under various applied positive potentials (Fig. 5a) for 1 h for releasing adsorbed Y(III) into 20 mM NaCl electrolyte. As depicted in Fig. 5a, P1-CNT exhibited almost full regeneration when applying +0.8 V during the first cycle desorption without using any acid or other stripping chemical additives. The successful adsorption and release of Y(III) on P1-CNT was also confirmed through X-ray photoelectron spectroscopy (XPS) (Fig. 5d) as well as scanning electron microscopy (SEM) and energy-dispersive spectroscopy (EDS) analyses (Section SI-7†), by monitoring the increase in yttrium content after adsorption, and its close to complete removal after electrochemical regeneration. Regeneration of P1-CNT was also tested with other REEs (Fig. 5c), with loaded P1-CNT releasing

Table 2 Estimated relative separation factors using P1-CNT electrodes

Ion A	Ion B	$\mathrm{RSF}_{A/B}$
Y^{3+}	Na^+	610.3 ± 6.33
Dy^{3+}	Y^{3+}	1.85 ± 0.087
Y^{3+}	Ce^{3+}	1.35 ± 0.046

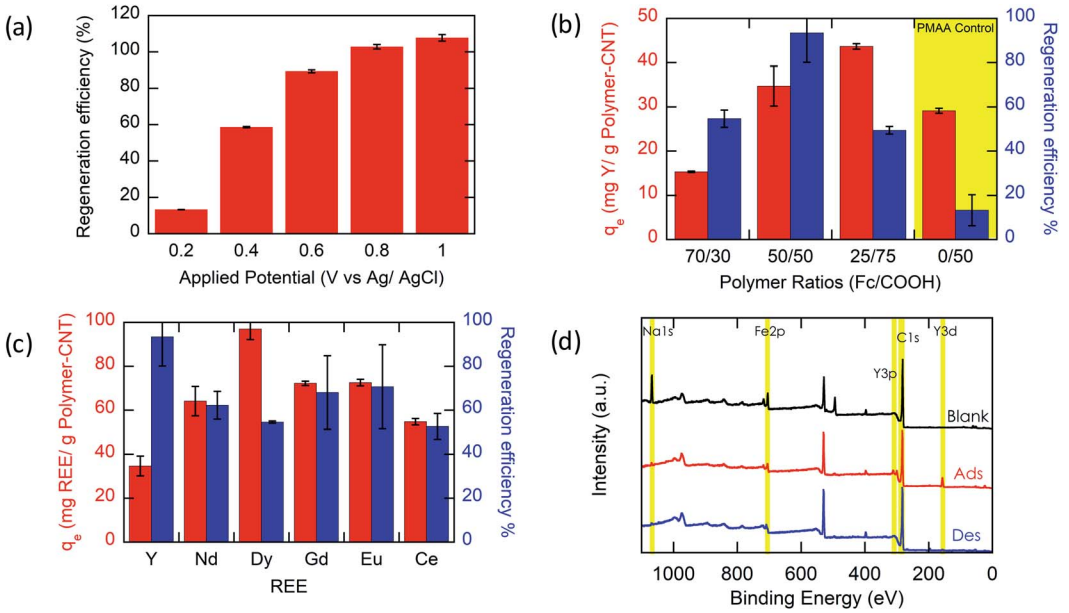

Fig. 5 The regeneration efficiency of REE ions. All adsorption prior to regeneration was conducted using standard adsorption parameters listed earlier (1 h, open circuit, 10 mL aqueous solution with 1 mM $RE(Cl)_3$ and 20 mM NaCl). All desorption conditions are as follows: 1 h, 10 mL aqueous solution with 20 mM NaCl. (a) Desorption of Y(III) from loaded P1-CNT electrodes at various applied potentials. (b) Adsorption/desorption of Y(III) with polymer-CNT electrodes with polymers having various ratios of ferrocenyl groups to carboxyl groups. Desorption with an applied potential of +0.8 V *vs.* Ag/AgCl. (c) REE uptake/regeneration efficiency using P1-CNT. (d) XPS surface analysis of P1-CNT before REE adsorption (blank), after Y(III) adsorption (Ads), and after Y(III) adsorption/desorption (Des).

adsorbed RE(III) into 20 mM NaCl upon applying +0.8 V for 1 h. Regeneration parameters for P1-CNT were set using Y(III) as the model for REE ions.

To prove the importance of the redox-active groups for release of REE ions, a copolymer with 52 mol% BzMA instead of FPMAm ($P(BzMA_{52}\text{-}MAA_{48})$, P5) was used, with BzMA being a non-redox control. P5-CNT showed a similar uptake to P1, but poor regeneration at 0.8 V (Fig. 5b), confirming that the redox-active ferrocene moieties are critical to promoting electrochemically regenerated release. Experiments varying the ratio of carboxylic acid to ferrocenyl groups showed that with increasing carboxylic acid group (binding site) content compared to ferrocene, desorption became less efficient (Fig. 5b), reaffirming the idea that the oxidation of ferrocene groups to ferrocenium cations is the driving force of the ion desorption process. XPS was used to estimate the ratio between reduced and oxidized ferrocene sites from the high-resolution Fe 2p spectra of the surface of P1-CNT (Fig. 6a–c). The oxidation degrees of Fe on the surface of pristine (or blank) P1-CNT and P1-CNT after adsorption of Y(III) in 1 mM YCl_3 and 20 mM NaCl for 1 h were similar to each other, with both showing that most of the Fc sites were in a reduced state. After regeneration (desorption) of the P1-CNT electrode *via* chronoamperometry at +0.8 V (*vs.* Ag/AgCl) in 20 mM NaCl for 1 h, over 70% of the Fc sites were oxidized. This result further suggests that the mechanism for desorption can be attributed to the oxidation of ferrocene.

Along with regeneration, reusability of the P1-CNT electrode is needed. As XPS analysis indicated in Fig. 6a–c, the number oxidized Fc^+ species increased after the application of positive potential during regeneration. To allow for sufficient uptake in the following cycles, the oxidized Fc^+ needs to be reduced back to Fc to start a new cycle of REE adsorption. Reducing the P1-CNT electrode completely is crucial to prevent excessive positive charges from repelling the REE cations, limiting the REE uptake.

The results of four adsorption–desorption cycles are shown in Fig. 6d. P1-CNT showed a minor decrease in uptake over 4 cycles but retained its regeneration efficiency. Desorption capabilities remained relatively constant over the course of the recycling runs, averaging around 80% recovery of the REE by electrochemical regeneration. Finally, an evaluation of energy integration and consumption for desorption was carried out (see Section SI-12 for calculation details†). We estimated that an energy consumption of about 79.3 kcal mol^{-1} Y was incurred for desorption at 0.8 V for 1 h. The use of lower potentials for oxidation showed lower energy consumption per mol of desorbed Y; however, these had significantly lower REE recovery, demonstrating that further process optimization can help decrease overall electricity consumption in the future, by improved selection of operational parameters. In parallel, molecular design of both ligands and redox-active groups can be expected to progressively increase the regeneration efficiency and reversibility.

4. Conclusions

In summary, we propose a new redox-copolymer as a promising proof-of-concept platform for electrochemically regenerated ion-exchange for REE recovery. Redox-copolymers

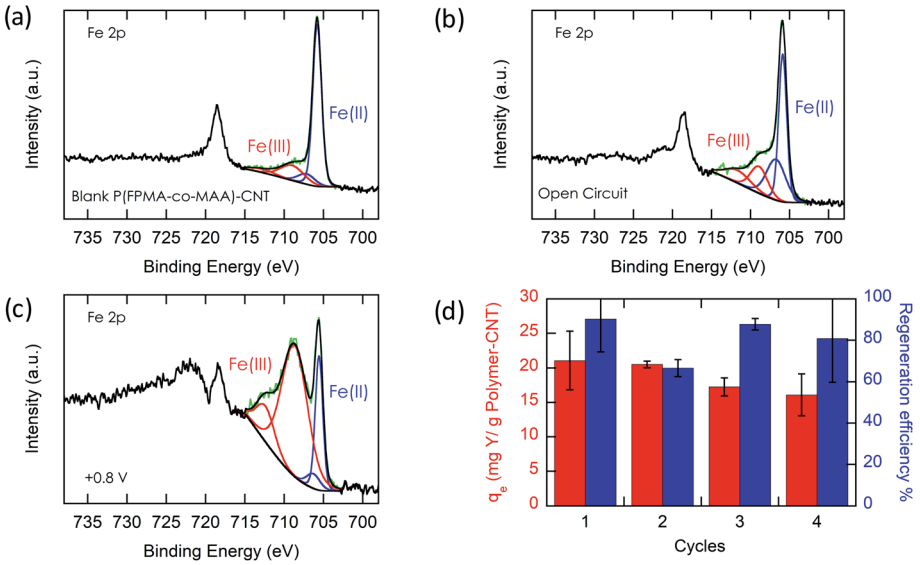

Fig. 6 High resolution Fe 2p spectra of the surface of P1-CNT at different stages of the adsorption/desorption process. (a) Pristine (blank) P1-CNT. (b) P1-CNT used for adsorption of Y(III) under the following conditions: 1 h, open circuit, 10 mL aqueous solution with 1 mM YCl_3 and 20 mM NaCl. (c) P1-CNT after adsorption of Y(III) regenerated (desorbed) for 1 h in 10 mL aqueous solution containing 20 mM NaCl with an applied potential of +0.8 V *vs.* Ag/AgCl. (d) Adsorption–desorption cycling runs using P1-CNT with adsorption of Y(III) under the following conditions: 1 h, open circuit, 10 mL aqueous solution with 1 mM YCl_3 and 20 mM NaCl and desorption for 1 h in 10 mL aqueous solution containing 20 mM NaCl with an applied potential of +0.8 V *vs.* Ag/AgCl.

containing carboxylic acid and ferrocene moieties were synthesized and studied for their effectiveness in recovery of REEs (Y, Nd, Eu, Gd, Dy, and Ce) from aqueous solutions. The copolymer showed increasing REE adsorption capacities with increasing content of MAA (the REE binding group), with a 50/50 ratio of ferrocenyl groups to carboxylic acid groups providing an optimal balance between uptake and electrochemical regeneration. Adsorption of Y(III) on P1-CNT showed an equilibrium capacity of 69.4 mg Y(III) per g polymer at an optimal pH of 6. Electrochemical desorption of the adsorbed REE from the electrodes was achieved using a positive potential *vs.* Ag/AgCl, to release the bound cation by electrostatic repulsion without the need for additional stripping reagents, achieving close to full regeneration under electrochemical conditions. The adsorption capacity of the recycled P1-CNT electrodes remained relatively constant during four consecutive cycles, confirming the structural stability of the redox-active copolymer. In conclusion, our work demonstrates that redox-copolymers can be a tunable functional material platform for electrochemically regenerable REE adsorption, providing modularity and sustainability to chemical adsorption systems, and pointing to future applicability in REE valorization from waste streams, chemical manufacturing separations, and even secondary recovery from various hydrometallurgical streams. We expect this fundamental concept of combining redox-groups with chemical ligands to be expanded to broader ion-exchange processes in the future.

Author contributions

H. V.: conceptualization, investigation, methodology, visualization, writing – original draft, writing – review and editing. J. E.: conceptualization, investigation, methodology, resources, visualization, writing – original draft, writing – review and editing. X. S.: conceptualization, project administration, supervision, writing – review and editing.

Conflicts of interest

There are no conflicts to declare.

Acknowledgements

This material is based upon work supported by the U.S. Department of Energy, Office of Science, Office of Basic Energy Sciences Separation Science program, under Award Number DE-SC0021409. The Q-Tof Ultima mass spectrometer was purchased in part with a grant from the National Science Foundation, Division of Biological Infrastructure (DBI-0100085). SEM and XPS characterizations were carried out in the Frederick Seitz Materials Research Laboratory Central Research Facilities, University of Illinois. The authors thank Angelique Klimek and Jing Lian Ng for their assistance with the experiments, Jemin Jeon for NMR measurements, and Dr Kwiyong Kim for assistance in energy calculations. The authors also thank Dr Roddel Remy for help with polymer characterization.

References

1 K. Binnemans, P. T. Jones, B. Blanpain, T. Van Gerven, Y. Yang, A. Walton and M. Buchert, *J. Clean. Prod.*, 2013, **51**, 1–22.
2 A. Chakhmouradian and F. Wall, *Elements*, 2012, **8**, 333–340.

3 B. S. Van Gosen, P. L. Verplanck, R. R. Seal Ii, K. R. Long and J. Gambogi, *Critical Mineral Resources of the United States—Economic and Environmental Geology and Prospects for Future Supply: U.S. Geological Survey Professional Paper Report 1802*, Reston, VA, 2017.
4 J. Gu, Z.-Q. Zhao, Y. Ding, H.-L. Chen, Y.-W. Zhang and C.-H. Yan, *J. Am. Chem. Soc.*, 2013, **135**, 8363–8371.
5 N. Davydov, R. Zairov, A. Mustafina, V. Syakayev, D. Tatarinov, V. Mironov, S. Eremin, A. Konovalov and M. Mustafin, *Anal. Chim. Acta*, 2013, **784**, 65–71.
6 N. A. Shamsutdinova, A. T. Gubaidullin, B. M. Odintsov, R. J. Larsen, V. D. Schepkin, I. R. Nizameev, R. R. Amirov, R. R. Zairov, S. N. Sudakova, S. N. Podyachev, A. R. Mustafina and A. S. Stepanov, *ChemistrySelect*, 2016, **1**, 1377–1383.
7 R. R. Zairov, N. A. Shamsutdinova, A. N. Fattakhova, A. V. Pyataev, A. F. Abdullin, A. V. Gerasimov, A. T. Gubaidullin and A. R. Mustafina, *Russ. Chem. Bull.*, 2016, **65**, 1325–1331.
8 N. A. Alarfaj and M. F. El-Tohamy, *J. AOAC Int.*, 2019, **99**, 380–385.
9 Q. Ju, D. Tu, Y. Liu, R. Li, H. Zhu, J. Chen, Z. Chen, M. Huang and X. Chen, *J. Am. Chem. Soc.*, 2012, **134**, 1323–1330.
10 N. Venkatachalam, T. Yamano, E. Hemmer, H. Hyodo, H. Kishimoto and K. Soga, *J. Am. Ceram. Soc.*, 2013, **96**, 2759–2765.
11 E. G. Moore, J. Xu, C. J. Jocher, E. J. Werner and K. N. Raymond, *J. Am. Chem. Soc.*, 2006, **128**, 10648–10649.
12 H.-X. Mai, Y.-W. Zhang, R. Si, Z.-G. Yan, L.-d. Sun, L.-P. You and C.-H. Yan, *J. Am. Chem. Soc.*, 2006, **128**, 6426–6436.
13 B. S. Van Gosen, P. L. Verplanck, K. R. Long, J. Gambogi and R. R. Seal Ii, *The Rare-Earth Elements: Vital to Modern Technologies and Lifestyles, Report 2014-3078*, Reston, VA, 2014.
14 U. S. G. Survey, *Mineral Commodity Summaries 2015*, U.S. Geological Survey, Reston, VA, 2015.
15 USGS, *Mineral Commodity Summaries 2020*, U.S. Geological Survey, 2020.
16 U. S. G. Survey, *Mineral Commodity Summaries 2021*, U.S. Geological Survey, Reston, VA, 2021.
17 E. Commission, *Report on Critical Raw Materials for the EU, Report of the Ad hoc Working Group on Defining Critical Raw Materials E. Commission*, European Commission, 2014.
18 U. S. D. O. Energy, *Critical Materials Strategy Summary*, U.S. Department of Energy, 2010.
19 U. S. D. O. Energy, *Critical Materials Strategy*, U.S. Department of Energy, 2011.
20 Y. Zhu, Y. Zheng and A. Wang, *Int. J. Biol. Macromol.*, 2015, **72**, 410–420.
21 I. Anastopoulos, A. Bhatnagar and E. C. Lima, *J. Mol. Liq.*, 2016, **221**, 954–962.
22 J. Song, T. Huang, H. Qiu, X. Niu, X.-M. Li, Y. Xie and T. He, *Desalination*, 2018, **440**, 18–38.
23 A. A. Galhoum, M. G. Mafhouz, S. T. Abdel-Rehem, N. A. Gomaa, A. A. Atia, T. Vincent and E. Guibal, *Nanomaterials*, 2015, **5**, 154–179.
24 F. Zhao, E. Repo, Y. Meng, X. Wang, D. Yin and M. Sillanpää, *J. Colloid Interface Sci.*, 2016, **465**, 215–224.
25 F. Wang, J. Zhao, X. Wei, F. Huo, W. Li, Q. Hu and H. Liu, *J. Chem. Technol. Biotechnol.*, 2014, **89**, 969–977.
26 M. Torab-Mostaedi, M. Asadollahzadeh, A. Hemmati and A. Khosravi, *Res. Chem. Intermed.*, 2015, **41**, 559–573.
27 J. Roosen, J. Spooren and K. Binnemans, *J. Mater. Chem. A*, 2014, **2**, 19415–19426.
28 J. Li, A. Gong, F. Li, L. Qiu, W. Zhang, G. Gao, Y. Liu and J. Li, *RSC Adv.*, 2018, **8**, 39149–39161.
29 X. Su, A. Kushima, C. Halliday, J. Zhou, J. Li and T. A. Hatton, *Nat. Commun.*, 2018, **9**, 4701.
30 K. Kim, S. Cotty, J. Elbert, R. Chen, C.-H. Hou and X. Su, *Adv. Mater.*, 2020, **32**, 1906877.
31 K. Kim, P. Baldaguez Medina, J. Elbert, E. Kayiwa, R. D. Cusick, Y. Men and X. Su, *Adv. Funct. Mater.*, 2020, **30**, 2004635.
32 R. Candeago, K. Kim, H. Vapnik, S. Cotty, M. Aubin, S. Berensmeier, A. Kushima and X. Su, *ACS Appl. Mater. Interfaces*, 2020, **12**, 49713–49722.
33 X. Su and T. A. Hatton, *Phys. Chem. Chem. Phys.*, 2017, **19**, 23570–23584.
34 P. D. Beer and P. A. Gale, *Angew. Chem., Int. Ed.*, 2001, **40**, 486–516.
35 X. Su, H. J. Kulik, T. F. Jamison and T. A. Hatton, *Adv. Funct. Mater.*, 2016, **26**, 3394–3404.
36 R. Chen, T. Sheehan, J. L. Ng, M. Brucks and X. Su, *Environ. Sci.: Water Res. Technol.*, 2020, **6**, 258–282.
37 R. Chen, J. Feng, J. Jeon, T. Sheehan, C. Rüttiger, M. Gallei, D. Shukla and X. Su, *Adv. Funct. Mater.*, 2021, 2009307.
38 M. Gallei and C. Rüttiger, *Chem.–Eur. J.*, 2018, **24**, 10006–10021.
39 R. Pietschnig, *Chem. Soc. Rev.*, 2016, **45**, 5216–5231.
40 P. S. Borchers, M. Strumpf, C. Friebe, I. Nischang, M. D. Hager, J. Elbert and U. S. Schubert, *Adv. Energy Mater.*, 2020, **10**, 2001825.
41 M. H. George and G. F. Hayes, *Polymer*, 1974, **15**, 397–400.
42 M. H. George and G. F. Hayes, *J. Polym. Sci., Polym. Chem. Ed.*, 1976, **14**, 475–488.
43 D. A. Baker, G. C. East and S. K. Mukhopadhyay, *J. Appl. Polym. Sci.*, 2001, **79**, 1092–1100.
44 H. Ni, H. Kawaguchi and T. Endo, *Colloid Polym. Sci.*, 2007, **285**, 819–826.
45 S. Azizian, *J. Colloid Interface Sci.*, 2004, **276**, 47–52.
46 I. Langmuir, *J. Am. Chem. Soc.*, 1918, **40**, 1361–1403.
47 S. J. Allen, G. McKay and J. F. Porter, *J. Colloid Interface Sci.*, 2004, **280**, 322–333.
48 H. Moon and W. Kook Lee, *J. Colloid Interface Sci.*, 1983, **96**, 162–171.